Multiscale Coarse-Graining of Ionic Liquids†

Yanting Wang, Sergei Izvekov, Tianying Yan,‡ and Gregory A. Voth*

Center for Biophysical Modeling and Simulation and Department of Chemistry, University of Utah, 315 South 1400 East Room 2020, Salt Lake City, Utah 84112-0850

Received: August 25, 2005; In Final Form: September 25, 2005

A recently developed multiscale coarse-graining (MS−CG) approach for obtaining coarse-grained force fields from fully atomistic molecular dynamics simulation is applied to the challenging case of the $EMIM^+NO_3^-$ ionic liquid. The force-matching in the MS−CG methodology is accomplished with an explicit separation of bonded and nonbonded forces. While the nonbonded forces are adopted from this force-matching approach, the bonded forces are obtained from fitting the statistical configurational data from the atomistic simulations. The many-body electronic polarizability is also successfully broken into effective pair interactions. With a virial constraint fixing the system pressure, the MS−CG models rebuild satisfactory structural and thermodynamic properties for different temperatures. The MS−CG model developed from a modest atomistic simulation is therefore suitable for simulating much larger systems, because the coarse-grained models show significant time integration efficiency. This approach is expected to be general for coarse-graining other ionic liquids, as well as many other liquid-state systems. The limitations of the present coarse-graining procedure are also discussed.

1. Introduction

Molten salts are liquid systems composed only of ions. Inorganic molten salts generally have a melting temperature much higher than room temperature. However, ionic liquids are a special kind of molten salts having a melting temperature around room temperature. This is generally achieved by employing a bulky asymmetric organic cation to prevent the ions from packing easily.[1] Although molten salts in general have been investigated for many decades,[2] only recently have ionic liquids drawn extensive attention and found possible industrial applications.[1,3,4] Due to their non-volatile behavior, the most attractive application of ionic liquids may be to replace the traditional volatile organic solvents, which are harmful to the environment. Other features, such as reusability, low viscosity, better reactivity and selectivity, also suggest that ionic liquids may be a good candidate to achieve the end goal of "green chemistry".

There are numerous ionic liquid systems[5] to be chosen from to meet specific requirements. However, despite the extensive experimental and theoretical studies in the past few years, current understanding of the physical and chemical properties of ionic liquids is still insufficient. One problem in theoretical studies is that bulky cations generally contain tens of atoms, which makes atomistic-scale computer simulations very expensive. Additionally, strong correlations between ions due to long-range Coulomb interactions require long time simulation. Furthermore, the many-body electronic polarizability, which has been found to have a significant influence on the properties of ionic liquid systems,[6,7] limits the simulation time step to less than 1 fs.

Coarse-grained (CG) models can provide extensive simulation data at a reasonable computational cost. In addition to the benefit of computational efficiency, it is also expected that the CG models can reveal the essential physical and chemical properties of ionic liquids by averaging over less important detailed information at the atomistic level. Several CG approaches have been developed to treat various kinds of chemical and biological systems (see, e.g., refs 8−15 and references therein). Generally speaking, coarse-graining is achieved by grouping atoms into fewer interaction sites. As a result, the major challenge is how to construct the effective force field between the CG sites. Typically, CG potentials of a preselected analytical form are parameterized either to match thermodynamic properties[8] or to reproduce average structural properties. The latter can be achieved by using an interactive adjustment of potential parameters, starting from an approximation based on potentials of mean force,[11,12] through the solution of the Ornstein−Zernicke equation,[13] or using the inverse Monte Carlo technique.[14,15] The applicability of these approaches may be limited by the preselected analytical forms for the CG potential, which usually has not been directly derived from the underlying atomistic interactions.

Recently, we have developed the alternative "multiscale coarse-graining" (MS−CG) approach[16,17] which is based on a force-matching (FM) method.[18−20] The MS−CG approach derives the effective force field between CG sites systematically from an underlying explicit atomistic molecular dynamics (MD) simulation by force-matching the coarse-grained image of atomistic trajectory and force data. It divides the radial distance between pairwise CG sites into bins and fits the force inside each bin individually, so that the generated force field is no longer restricted to a simple analytical form for the range of its radial distance.

In this work the MS−CG approach is applied to coarse-grain the polarizable atomistic model[6,7] of the 1-ethyl-3-methylimidazolium nitrate ($EMIM^+NO_3^-$) ionic liquid system. A force-matching with explicit separation of bonded and nonbonded interactions is used. A method is then introduced to refine

† Part of the special issue "Michael L. Klein Festschrift".

* To whom correspondence should be addressed. Phone: (801)581−7272. Fax: (801)581−4353. E-mail: voth@chemistry.utah.edu.

‡ Current address: Institute of New Energy Material Chemistry, Nankai University, Tianjin 300071, China.

10.1021/jp0548220 CCC: $33.50
Published on Web 11/04/2005

bonded force field parameters from the atomic configuration data. It will be shown that, upon application to the ionic liquid system, the MS−CG approach maps the many-body polarizability into effective pair potentials and leads to CG models that provide satisfactory structural properties for different temperatures. With the system virial also built in, thermodynamic properties can additionally be reproduced by the CG models with good accuracy. The bonded parameters are found to be transferable to different temperatures, but the nonbonded effective potentials are less so because they are approximate site−site potentials of mean force (PMF) for the given thermodynamic conditions. The errors in the structural properties and the nontransferability between temperatures can be largely attributed to the isotropic CG representation of anisotropic atomistic structures, making the site−site PMF quite different at different temperatures. However, it will be shown that the MS−CG models are well transferable to different system sizes. The MS−CG models can easily simulate a system about 200 times larger than the polarizable atomistic model for a given amount of CPU time. The MS−CG method is expected to be suitable for other ionic liquids, as well as many other organic chemical systems.

The structure of this paper is as follows. In section 2 the nonpolarizable and the polarizable atomistic ionic liquid models are described, along with the method of retrieving bonded force field parameters from the configurations and the FM method for the nonbonded interactions. Section 3 reports the details of the coarse-graining and force-matching procedures applied to the $EMIM^+NO_3^-$ ionic liquid system, as well as the comparison of the structural and thermodynamic properties between the atomistic and the CG simulations. Conclusions are then given in section 4.

2. Models and Methods

In this section the nonpolarizable and the polarizable atomistic models for the $EMIM^+NO_3^-$ ionic liquid are first described, followed by the systematic development of the CG models for ionic liquids, based on the underlying atomistic simulations. The nonbonded interactions are first obtained by the FM method with explicit separation of bonded and nonbonded forces. The parameters for the bonded interactions are then defined by directly retrieving statistical data from the saved atomistic MD configurations.

2.1. Atomistic Models. A nonpolarizable atomistic model for ionic liquids[21] can be expressed as an empirical force field potential V_{np} with a bonded part V_b and a nonbonded part V_{nb}, such that

$$V_{np} = V_b + V_{nb} \tag{1}$$

The term V_b generally has the typical bond, valence angle, and dihedral angle terms among atoms. One widely used choice for ionic liquids[21−24] has harmonic terms for bonds and valence angles, and cosine terms for dihedral angles, i.e.,

$$V_b = \sum_{\text{bonds}} \frac{1}{2} k_r (r - r_0)^2 + \sum_{\text{angles}} \frac{1}{2} k_\theta (\theta - \theta_0)^2 + \sum_{\text{dihedrals}} V_n \cos(n\phi - \gamma) \tag{2}$$

where k_r, k_θ, V_n are force constants, r, θ, ϕ are bond, valence angle, and dihedral angle, respectively, r_0, θ_0, and γ are equilibrium positions, and n is an integer number.

The nonbonded potential V_{nb} contains the short-range van der Waals potentials V_{VDW} and the long-range Coulomb contributions V_{el} between nonbonded atoms, given by

$$V_{nb} = V_{VDW} + V_{el} \tag{3}$$

The van der Waals interactions generally take the 12−6 Lennard-Jones potential form,

$$V_{VDW} = \sum_i \sum_{j>i} 4\epsilon \left[\left(\frac{\sigma}{r_{ij}} \right)^{12} - \left(\frac{\sigma}{r_{ij}} \right)^{6} \right] \tag{4}$$

where ϵ is the depth of the energy minimum, σ is the minimum energy distance, r_{ij} is the distance between atom i and atom j. In the Coulomb potentials, the charge q_i on atom i is the partial charge including the permanent dipole effect. The partial charges can be obtained from an ab initio study of the ions, satisfying the constraint $\Sigma_i q_i = 1$ for cation, and $\Sigma_i q_i = -1$ for anion. With those partial charges, the Coulomb potential is written as

$$V_{el} = \sum_i \sum_{j>i} \frac{q_i q_j}{r_{ij}} \tag{5}$$

Recently Yan et al.[6,7] developed a polarizable model for ionic liquids. Rather than using the simpler but much slower dipole iteration method, a fast extended Lagrangian approach[25] similar in spirit to the Car−Parrinello method[26] has been used to treat the many-body polarizable model. In this method the induced dipole degrees of freedom are coupled to a heat bath with a very low temperature (∼0.1 K) separated from the system heat bath to help keep them evolving on the adiabatic surface. Despite the increased simulation time (about a factor of 2), the polarization caused by the induced dipoles has been shown[6,7] to have a significant influence on both the structural and the dynamical properties of ionic liquids. The polarizable model also brings the atomistic simulation results into closer agreement with the experimental data.[6,7]

In the polarizable model, an induction term V_{ind} is added to the nonpolarizable potential V_{np}. The total potential of the polarizable model is therefore given by

$$V_{pol} = V_{np} + V_{ind} \tag{6}$$

with V_{ind} expressed as

$$V_{ind} = -\sum_i \boldsymbol{\mu}_i \cdot \mathbf{E}_i^0 - \sum_i \sum_{j>i} \boldsymbol{\mu}_i \cdot \mathbf{T}_{ij} \cdot \boldsymbol{\mu}_j \sum_i + \frac{\boldsymbol{\mu}_i \cdot \boldsymbol{\mu}_i}{2\alpha_i^2} \tag{7}$$

In the above equation $\mathbf{E}_i^0 = \Sigma_{j\neq i} q_j \mathbf{r}_{ij}/r_{ij}^3$ is the electric field on atom i, generated by the partial charges of all other atoms, excluding those within the same ion of atom i. The dipole field tensor $\mathbf{T}_{ij}$ is calculated from the electrostatic potential $\phi^f(|\mathbf{r}_i - \mathbf{r}_j|)$ at point j due to the charge at point i: $\mathbf{T}_{ij} = \nabla_i \nabla_i \phi^f(|\mathbf{r}_i - \mathbf{r}_j|)$. The induced dipole moment is $\boldsymbol{\mu}_i = \alpha_i[\mathbf{E}_i + \Sigma_{j=1,j\neq i}^N \mathbf{T}_{ij} \cdot \boldsymbol{\mu}_j]$, where α_i is the atomic polarizability of atom i, $\mathbf{E}_i$ is the electric field on atom i. The isotropic atomic polarizabilities $\{\alpha_i\}$ are determined by fitting the anisotropic molecular polarizabilities of the ions, which can be obtained by ab initio simulation. Note that all of the terms in V_{np} are pair potentials, but the induced dipole on each atom depends on the positions of all atoms, so the polarizability is a many-body effect.

2.2. Force-Matching Method for Nonbonded Interactions. The coarse-graining of ionic liquids involves a reduction in the number of interaction sites inside of each ion. The center of a

CG site can be taken to be the center-of-mass of the underlying atoms. A group of atoms can be most readily coarse-grained as one site if there are relatively few degrees of freedom inside that group. For example, an aromatic ring can be considered as one CG site because its backbone structure is almost a rigid body. A methyl group can also be one CG site because in many cases it rotates along its principal axis symmetrically. The anion of ionic liquids is also generally small and amenable to coarse-graining as a single CG site. By contrast, the atoms of the bulky cation generally have to be grouped into several CG sites, connected by new intramolecular bonds and angles at the CG level. In our previous MS−CG work,[16,17] bonded and nonbonded interactions were mixed together, with the bond force field parameters being decided according to the matched force, and the angles were treated as harmonic bonds. This approach works well for the bonds, but for ionic liquids treating the valence and dihedral angles as harmonic bonds may not be a good approximation. A different approach of obtaining the bonded parameters will therefore be introduced in section 2.3, and the FM procedure described below will be applied only to the nonbonded CG sites.

A new FM method[18] is the basis of the MS−CG approach. This FM method is an extension of the least-squares FM approach originally suggested by Ercolessi and Adams.[27] It can determine a pairwise effective force field from given trajectory and force data regardless of their origin, e.g., ab initio MD simulation,[18] path-integral MD simulation,[20] or coarse-graining of atomistic MD simulation.[16,17] With the FM methodology, the many-body polarization effects are also able to be represented by pairwise effective potentials.

In the MS−CG methodology, the atoms are first grouped into CG sites, with the CG force on a CG site α being the net force on all underlying atoms, $\mathbf{F}_\alpha^{\mathrm{cg}} = \Sigma_i \mathbf{f}_\alpha^{\,i}$, where $\mathbf{f}_\alpha^{\,i}$ is the force on the ith underlying atom. The pairwise effective force $\mathbf{f}^{\mathrm{p}}(r_{ij})$ between CG sites i and j is represented as the sum of a short-range part and a long-range Coulomb part, i.e.,

$$\mathbf{f}^{\mathrm{p}}(r_{ij}) = -\left(f(r_{ij}) + \frac{Q_i Q_j}{r_{ij}^{\,2}}\right)\mathbf{n}_{ij} \tag{8}$$

where r_{ij} is the modulus of the vector $\mathbf{r}_{ij} = \mathbf{r}_i - \mathbf{r}_j$ connecting the two CG sites, Q_i is the partial charge of CG site i, and $\mathbf{n}_{ij} = \mathbf{r}_{ij}/r_{ij}$. The short-range term $f(r_{ij})$ is represented by third-order polynomials (cubic splines)[28] connecting a set of points $\{r_k\}$ (which meshes the interatomic separation up to the cutoff radius $r_{k_{\max}}$), thus preserving continuity of its functions and their first two derivatives across the junction such that

$$f(r,\{r_k\},\{f_k\},\{f_k''\}) = A(r,\{r_k\})f_i + B(r,\{r_k\})f_{i+1} + C(r,\{r_k\})f_i'' + D(r,\{r_k\})f_{i+1}'' \tag{9}$$

where $r \in [r_i, r_{i+1}]$, A, B, C, and D are known functions of r, $\{r_k\}$, $\{f_k\}$, and $\{f_k''\}$ are tabulations of $f(r)$ and its second derivatives on a radial mesh grid $\{r_k\}$. A key property for the success of this method is that a spline representation depends *linearly* on its parameters, which are tabulations of $f(r)$ and its second derivative, $\{f_k, f_k''\}$, on a radial mesh $\{r_k\}$. The parameters $\{f_k, f_k''\}$ are obtained from the fit.

Equalization of the atomistic MD forces $\mathbf{F}_{il}^{\mathrm{cg}}$ to forces predicted by using the representation in eqs 8 and 9, which act on the ith CG site in the lth configuration sampled along the atomistic trajectories, results in the following set of linear equations

$$-\sum_{\gamma=\mathrm{nb,b}}\sum_{\beta=1,Kj=1,N_\beta}\sum\left(f\{r_{\alpha il,\beta jl}\},\{r_{\alpha\beta,\gamma,k}\},\{f_{\alpha\beta,\gamma,k}\},\{f''_{\alpha\beta,\gamma,k}\} + \frac{Q_{\alpha\beta}}{r_{\alpha il,\beta jl}^{\,2}}\delta_{\gamma,\mathrm{nb}}\right)\mathbf{n}_{\alpha il,\beta jl} = \mathbf{F}_{\alpha il}^{\mathrm{cg}} \tag{10}$$

with respect to the force parameters subject to the fit $\{f_{\alpha\beta,\gamma,k}, f''_{\alpha\beta,\gamma,k}, Q_{\alpha\beta}\}$, where $\alpha = 1, \cdots, K$, $i = 1, \cdots, N_\alpha$. In eqs 10, $\{\alpha il\}$ labels the ith atom of kind α in the lth configuration; $r_{\alpha il,\beta jl}$ is the distance between atoms $\{\alpha i\}$ and $\{\beta j\}$ in the lth configuration; $Q_{\alpha\beta} = Q_\alpha Q_\beta$ with Q_α the partial charge of the CG sites of kind α; N_β and K are, respectively, the number of the CG sites of kind β and the total number of kinds of CG sites in the system.

The method also permits systematic separation of bonded and nonbonded CG forces. This is important for the sites which have an overlap in regions of intra- and intermolecular motion, causing the FM force field to be a mixture of bonded and nonbonded components, which then become impossible to separate for these regions. To explicitly fit the bonded forces, the additional index $\gamma = \{\mathrm{nb,b}\}$, which indicates whether the site pair αil, βjl is bonded (i.e., $\gamma = \mathrm{b}$), is used to distinguish the f, f'' parameters in eqs 10 for bonded and nonbonded interactions. For bonded pairs the Coulomb term is absent, which is enforced by the $\delta_{\gamma,\mathrm{nb}}$ term which is unity if $\gamma = \mathrm{nb}$, and zero otherwise. It will be assumed that in eqs 10 the index l runs over a sufficiently large number of the configurations L such that the equations overdetermine the force parameters. Standard equations which are linear with respect to $\{f_{\alpha\beta,\gamma,k}, f''_{\alpha\beta,\gamma,k}\}$ must also be included in eqs 10 to ensure that the first derivative of $f(r)$ is continuous across the boundary between two intervals.[28]

The MS−CG force fields described above perform well in reproduction of the structural properties; however, in some cases they fail to maintain the proper internal pressure in the system, and as a result the density can be wrong (too low) in constant NPT simulations. This behavior is attributed to two primary reasons which can be seen from the virial equation used to evaluate the pressure in MD simulation, i.e.,

$$P = \left(\frac{2}{3}\langle E^{\mathrm{kin}}\rangle + \langle W\rangle\right)/V \tag{11}$$

where

$$\langle E^{\mathrm{kin}}\rangle = Nk_{\mathrm{B}}T/2 \tag{12}$$

is the average kinetic energy and

$$\langle W\rangle = \left\langle \frac{1}{3}\sum_{i<j}\mathbf{f}_{ij}\cdot\mathbf{r}_{ij}\right\rangle \tag{13}$$

is the virial of the system. In eq 12 N is the number of system degrees of freedom and T is the system temperature. As seen from eq 12, because the coarse-graining of the system eliminates some degrees of freedom, the first term in eq 11 is lower compared to atomistic simulation and therefore so is the pressure P. The second reason for an inaccurate density from MS−CG models is related to the second (virial) term in eq 11. The coarse-graining of the system does not preserve the virial term. In particular, it contracts the system virial of contributions of forces which are "intra" with respect to the atomic groups subject to coarse-graining. Fortunately, because the virial $\langle W\rangle$ depends linearly on the atomic forces and E^{kin} does not rely on the forces at all, the FM force field can be constrained to produce the

correct pressure. This task can be accomplished by adding to eqs 10 the constraint

$$\sum_{\gamma=\mathrm{nb,b}} \sum_{\substack{\alpha=1,Ki=1,N_\alpha \\ \beta=1,Kj=1,N_\beta}} \sum \left(f(r_{\alpha il,\beta jl},\{r_{\alpha\beta,\gamma,k}\},\{f_{\alpha\beta,\gamma,k}\},\{f''_{\alpha\beta,\gamma,k}\}) r_{\alpha il,\beta jl} + \frac{Q_{\alpha\beta}}{r_{\alpha il,\beta jl}} \delta_{\gamma,\mathrm{nb}} \right) = 3W_l^{\mathrm{atm}} + 2\Delta E^{\mathrm{kin}} \quad (14)$$

where W_l^{atm} is the "instantaneous" virial for the lth configuration along the atomistic trajectories, and

$$\Delta E^{\mathrm{kin}} = E_l^{\mathrm{kin,atm}} - E_l^{\mathrm{kin,CG}} \quad (15)$$

In eq 15, $E_l^{\mathrm{kin,atm}}$ and $E^{\mathrm{kin,CG}}$ are the "instantaneous" kinetic energies for the lth configuration along atomistic trajectories and its CG representation, respectively. The difference ΔE^{kin}, which accounts for the change in pressure due to the reduction in system degrees of freedom, can be calculated less accurately, but more conveniently, as

$$\Delta E^{\mathrm{kin}} = E_l^{\mathrm{kin,atm}}(1 - N^{\mathrm{CG}}/N^{\mathrm{atm}}) \quad (16)$$

where N^{atm} and N^{CG} are numbers of degrees of freedom of the atomistic and CG systems, respectively.

The fitted data in eqs 14 depend explicitly on the instantaneous kinetic energy and, therefore, on the temperature in the reference atomistic simulation. This may further reduce the transferability of the MS−CG models to other temperatures. In particular, thermodynamic properties which rely on the derivatives of the temperature (e.g., thermal expansion coefficient) may be less accurate. However, this is not a serious issue because the MS−CG potential can be readily refit for different thermodynamic conditions, as will be demonstrated later.

Because of the limited number of fitted atomistic MD configurations, the matched nonbonded forces contain some statistical noise that makes the force profiles somewhat rough. The roughness can be smoothed out by using a least-squares fit with a proper set of analytical functions. For ionic liquids, the matched nonbonded forces are usually quite regular, so a polynomial function is more than adequate for the least-squares fit of the spline data in eq 9, i.e.,

$$f_{ij}(r) = \sum_{n=2}^{M} A_{ij}^{\,n}/r^n \quad (17)$$

where $f_{ij}(r)$ is the short-range term of the matched force between the CG sites i and j defined in eq 8, r is the radial distance, A_{ij}^n is the coefficient for the nth polynomial item, M is the highest order of the power. For the $EMIM^+NO_3^-$ ionic liquid, $M = 16$ is found to provide good accuracy.

For systems with no more than 3 sites, e.g., water[18] and hydrogen fluoride,[19] the partial charges $\{Q_\alpha\}$ can be recovered by solving the nonlinear equations $Q_{\alpha\beta} = Q_\alpha Q_\beta$ with $Q_{\alpha\beta}$ obtained from eqs 10. For CG models of ionic liquids, which generally contain more than 3 CG sites, it is more difficult to solve the partial charges explicitly from eqs 10. Fortunately, the partial charge of each CG site can be simply fixed to be the sum from the underlying atoms in the atomistic representation, i.e.,

$$Q_\alpha = \Sigma_i q_{\alpha i} \quad (18)$$

Equation 18 works as a constraint in addition to eqs 14 to solve eqs 10. This approximation introduces two sources of error into the effective long-range interaction. First, the dipole and higher electrical moments caused by the finite distribution of underlying atomic charges on the CG site are neglected. Second, the weak long-range many-body polarization effects of the CG site are not included in the long-range Coulomb part in eq 8. For a fixed size of periodic boundary box for which the MS−CG procedure is used, this approximation does not introduce significant error into the CG results, because the above interactions are captured by the short-range part in eq 8. It may make a difference only when the MS−CG model is constructed from a smaller atomistic MD system and then used to simulate a system at a significantly larger size. Fortunately, this seems to not be a serious problem in practice, because both are weak long-range effects.

It should be noted that the effective CG potentials, constructed by the FM or any other approach intended to reproduce structural properties, are actually a many-body site−site PMF. The vibrational potentials among different CG groups are averaged out. Although the resulting PMF may reproduce the structural properties accurately, the neglect of vibrational potentials and the reduced number of system degrees of freedom will cause any CG model to exhibit a faster diffusion.[19,29] Further methodological development is therefore necessary to yield accurate dynamical properties. One possible approach is coupling fictitious harmonic oscillators to the CG sites according to the generalized Langevin equation (see, e.g., ref 30). The diffusion of the CG sites will then be reduced without changing the underlying liquid structure. In this paper, however, only the structural and the thermodynamic properties of the MS−CG models for ionic liquids are presented. The dynamical properties of the MS−CG model will be the subject of future investigation.

Another general problem that influences the structural properties of CG models is that each CG site has been treated as an isotropic sphere. That is, the CG potentials of mean force depend only on their radial distance, not their mutual orientation. However, the atomistic potentials between atomic groups generally depend on the mutual spatial orientation. A matched CG force $\mathbf{f}^{\mathrm{p}}(r_{ij})$ is therefore effectively averaged over the spatial orientations, i.e.,

$$\mathbf{f}^{\mathrm{p}}(r_{ij}) = \int P(\Omega_{ij}) \mathbf{f}^{\mathrm{p}}(r_{ij},\Omega_{ij})\, \mathrm{d}\Omega_{ij} \quad (19)$$

where Ω_{ij} is the relative spatial angle between two CG sites i and j, $\mathbf{f}^{\mathrm{p}}(r_{ij},\Omega_{ij})$ is an orientation-dependent mean force, and $P(\Omega_{ij})$ is the normalized probability distribution of Ω_{ij}. Such an approximation may be significant, so in the following sections this will be referred to as the "anisotropy effect".

2.3. Bonded Coarse-Grained Force Field Parameters. The FM method allows one to explicitly separate the bonded and nonbonded forces. The bonded forces are needed to describe interactions between bonded CG site pairs in a CG MD simulation. All bonds might be described at the simplest level by harmonic potentials. In principle, the harmonic bonded potentials can then be obtained through least-squares fit of the FM bonded forces to a harmonic force (i.e., by a linear function). However, as seen from Figure 1, the CG bonded forces for ionic liquids often deviate from being harmonic, and some further generalizations are required. Therefore, in the present work a systematic and accurate way of retrieving effective bonded force field parameters from the saved MD configurations is described. This new approach is based on an existing method applied by several other authors,[31−33] but a further refinement of the method leads to better accuracy. An example is given below by applying the method to a bond interaction, but it is also valid for the

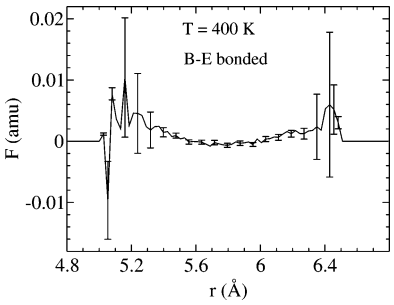

Figure 1. Matched bonded force by the FM approach between CG sites B and E (shown in Figure 2b). The error bars are the standard deviations. By contrast, a harmonic force would be linear with a constant slope.

valence and dihedral angles. The only difference is the choice of the functional forms of the potentials for the different classes of bonded interactions.

If an *isolated* bond with a bond potential $V_b(r)$ is in the canonical ensemble, with r being the bond length, then the probability $P(r)$ of r obeys the Boltzmann distribution

$$P(r) = C \exp(-V_b(r)/k_B T) \tag{20}$$

where C is a constant, k_B is Boltzmann's constant, and T is the designated system temperature, which is a constant in the canonical ensemble. The distribution $P(r)$ of the bond length r can be obtained from the configurations saved during the atomistic MD simulation. With an appropriate functional form of $V_b(r)$ assumed, its parameters are determined by fitting $P(r)$ according to eq 20.

The above procedure has been employed by others,[31−33] where the isolated system parameters are first obtained and used as the input to the condensed phase CG simulations. However, the above procedure is incomplete. Since the bond in a condensed phase system is not isolated, the parameters thus obtained may deviate from the actual equilibrium parameters due to the environment. Suppose $\mathcal{F}$ is the functional representing the effect of the interaction with the environment. Near equilibrium it is assumed that this functional does not change the functional form of the bond, but only the parameter values of the functional. Now suppose A_0 is the parameter set at equilibrium, and A_1 is the apparent fitted set obtained by the described procedure in the previous paragragh, then $\mathcal{F}\{V_b(A_0,r)\} = V_b(A_1,r)$. Now the question is how, with an appropriate assumed functional form $V_b(A,r)$ and a set of apparent fitted parameters A_1, one determines the actual desired set A_0, or equivalently, the functional $\mathcal{F}$.

If it is first assumed that, near equilibrium, the functional $\mathcal{F}$ does not change in the simulations with different set of parameters, then $\mathcal{F}$ can be determined from a further CG run. By performing a CG run using the obtained set of parameters A_1 (presuming the nonbonded interactions have already been determined by the procedure described in section 2.2), the fitting of the resulting CG configurations gives another set of parameters A_2. $\mathcal{F}$ is then determined from these two known sets, $\mathcal{F}\{V_b(A_1,r)\} = V_b(A_2,r)$. Once $\mathcal{F}$ is known, the desired set A_0 can be determined by $V_b(A_0,r) = \mathcal{F}^{-1}\{V_b(A_1,r)\}$.

For example, given a harmonic bond potential $V_b(r) = 1/2\, k_r(r - r_0)^2$, the set of parameters from the atomistic configurations is $A_1 = \{k_r^1, r_0^1\}$, that from the subsequent CG run is $A_2 = \{k_r^2, r_0^2\}$, so then

$$\mathcal{F}\{V_b(r)\} = \{k_r \rightarrow c_k k_r,\ r_0 \rightarrow c_r + r_0\} \tag{21}$$

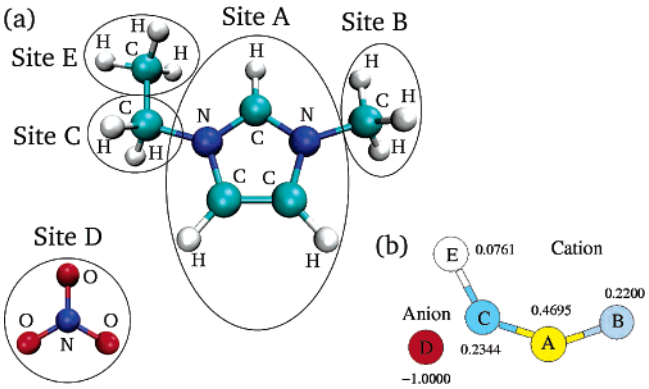

Figure 2. (a) Atomic structure of the $EMIM^+NO_3^-$ ionic liquid. (b) Coarse-grained $EMIM^+NO_3^-$ ionic liquid structure. The numbers shown on the CG sites are their partial charges.

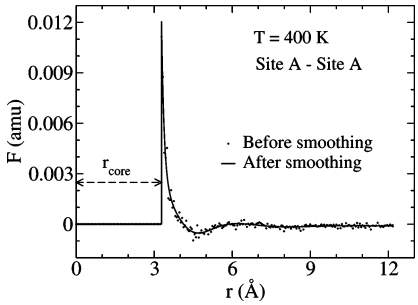

Figure 3. Matched force of CG sites A−A at $T = 400$ K before and after smoothing out by the polynomial function in eq 17.

where $c_k = k_r^1/k_r^2$, and $c_r = r_0^1 - r_0^2$. This determines the desired CG set

$$A_0 = \{k_r^0 = c_k k_r^1 = (k_r^1)^2/k_r^2,\ r_0^0 = c_r + r_0^1 = 2r_0^1 - r_0^2\} \tag{22}$$

No systematic way has been established to determine the actual best functional form $V_b(r)$ for the bonded interactions. In a practical sense, several possible forms may be fitted to the distribution $P(r)$ from the atomistic MD simulation to see which one yields the best fit. The results in section 3.1 will show that, for the present system being studied, this method is complete and accurate.

3. Results and Discussion

In this section the MS−CG procedure is applied to construct CG models for the $EMIM^+NO_3^-$ ionic liquid system at two different temperatures, $T = 400$ and 700 K. The experimental melting temperature of this liquid is ~313 K.[34] The CG simulations are then compared with the results of atomistic MD simulations for different sizes. The DL_POLY program[35] was used to perform the MD simulations for both the atomistic and the CG models. Periodic boundary conditions were employed within a cubic cell. The long-range charge−charge, charge−dipole, and dipole−dipole interactions were treated using the Ewald sum.[36] The system was coupled to either a Nosé-Hoover thermostat[37] for the constant NVT ensemble or a Hoover barostat[38] for the constant NPT ensemble. Another Nosé-Hoover thermostat or Hoover barostat with a very low temperature of $T = 0.1$ K was used for the induced dipole degrees of freedom to treat the electronic polarizability.[6,7] A cutoff of 12.17 Å was applied to the short-range interactions.

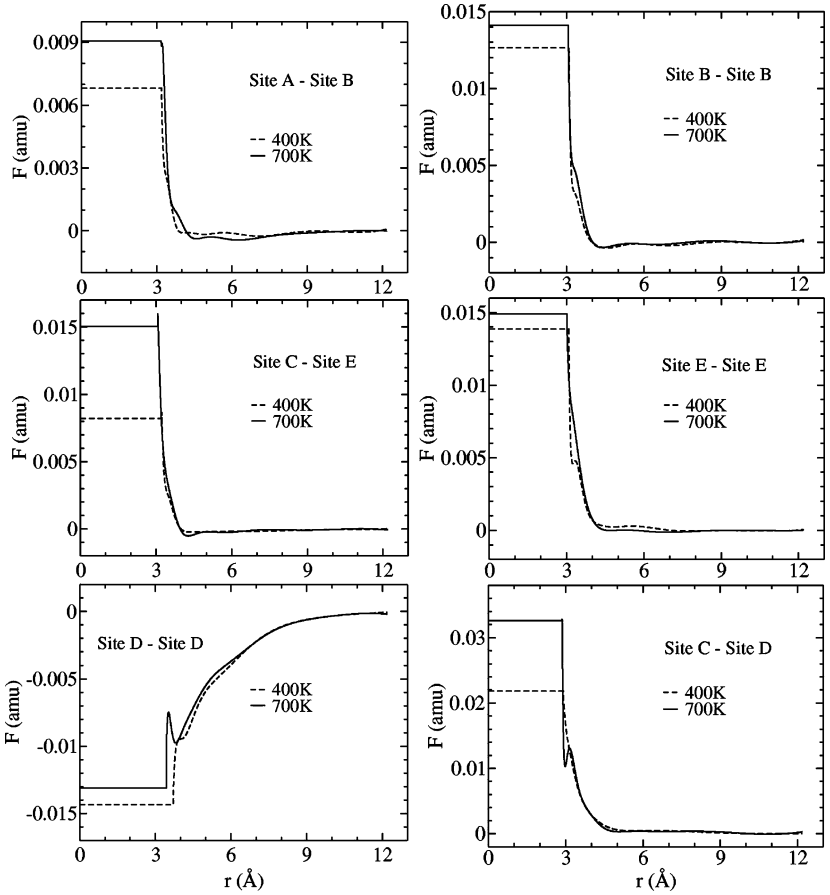

Figure 4. Matched short-range nonbonded forces between CG sites at $T = 400$ K (dashed lines) and 700 K (solid lines). Only six out of fifteen possible site−site forces are shown. Most of the forces are different for the two temperatures, indicating that the nonbonded forces have limited transferability between temperatures.

The choice of $T = 400$ K is based on the fact that $EMIM^+NO_3^-$ has been studied extensively at this temperature by MD simulations with both nonpolarizable[22] and polarizable[6,7] atomistic models. The results at a higher temperature of $T = 700$ K are compared here with those at $T = 400$ K to demonstrate that the MS−CG approach works well for different temperatures, and also that the major error of the present CG model comes from the anisotropy effect described in section 2.2. Although experimentally 700 K might be higher than the decomposition temperature of $EMIM^+NO_3^-$, it is not an issue with the present MD simulations, because the intramolecular bonds in the atomistic-level force field are not allowed to break. The higher temperature results are to be taken as illustrative results only.

3.1. Coarse-Graining and Force-Matching Procedures. As stated earlier, the $EMIM^+NO_3^-$ ionic liquid has been studied with both nonpolarizable[22] and polarizable[6,7] atomistic models at $T = 400$ K. The Amber force field parameters[39] have been used in these models. While both models have yielded satisfactory results, the results for the polarizable model are closer to the experimental data, demonstrating that electronic polarizability can play an important role in ionic liquid systems. Figure 2a shows the atomic structures of the $EMIM^+$ cation and the NO_3^- anion. The atomic polarizabilities reported in ref 7 have been adopted in this work. The force field parameters and the atomic polarizabilities are listed in the Supporting Information.

For the MS−CG models, the atoms have been grouped into 5 CG sites, as illustrated in Figure 2a. The resulting structure of the MS−CG models is shown in Figure 2b. This CG structure is designed so that the number of CG sites is as few as possible, but also with no significant degrees of freedom inside of each CG site. Because the anion and the backbone of the aromatic ring in the cation are almost rigid bodies, each of them has been considered as one CG site (Site A as the aromatic ring, site D as the anion). As the methyl group and the two methylene groups are rotationally symmetric to their principal axes, they have been coarse-grained as sites C, B, and E, respectively. For the CG cation, there are three bonds (A−B, A−C, and C−E), two valence angles (B−A−C and A−C−E), and one dihedral angle (B−A−C−E).

An atomistic-scale $EMIM^+NO_3^-$ system with 64 ion pairs under cubic periodic boundary conditions was first equilibrated with the polarizable atomistic model in the constant NPT ensemble at a temperature of $T = 400$ K and a pressure of $P = 1$ atm. The presence of polarizability limited the time step to 0.45 fs. The system size of 64 ion pairs was chosen because it is small enough for easy manipulations of the force-matching equations, while still large enough so that the pairwise effective short-range interactions are well sampled up to the point where the force can be truncated as 0.

The system was then simulated using a constant NVT ensemble at $T = 400$ K, with the volume set to be the average volume obtained from the constant NPT run, $V = a^3$, where $a = 25.0155$ Å is the side length of the boundary cube. After equilibration, 3×10^6 MD time steps were simulated, propagating the system for a total of 1.35 ns. During the simulation, a total of 4000 configurations were evenly sampled with an interval of 750 steps. In each configuration, the system virial,

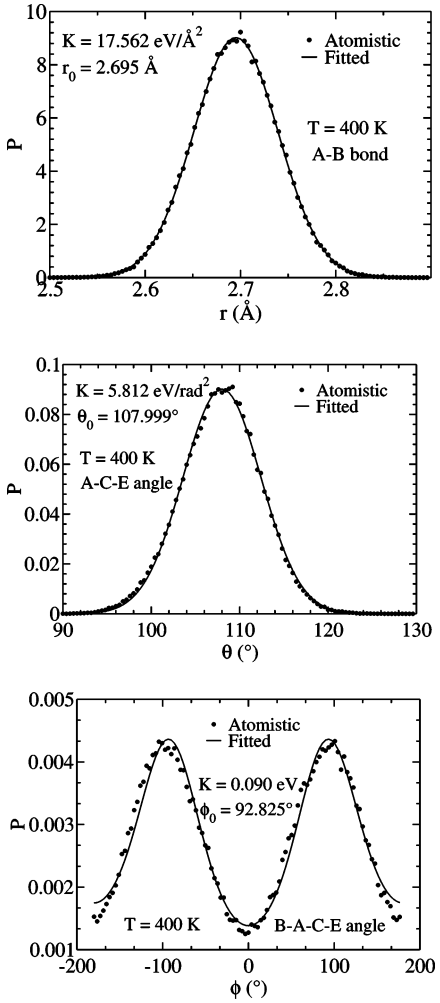

Figure 5. Bond and angle distributions (dotted lines) from the atomistic MD simulation and their fits (solid lines). Only the A−B bond, the A−C−E angle, and the dihedral angle are shown. Others are similar.

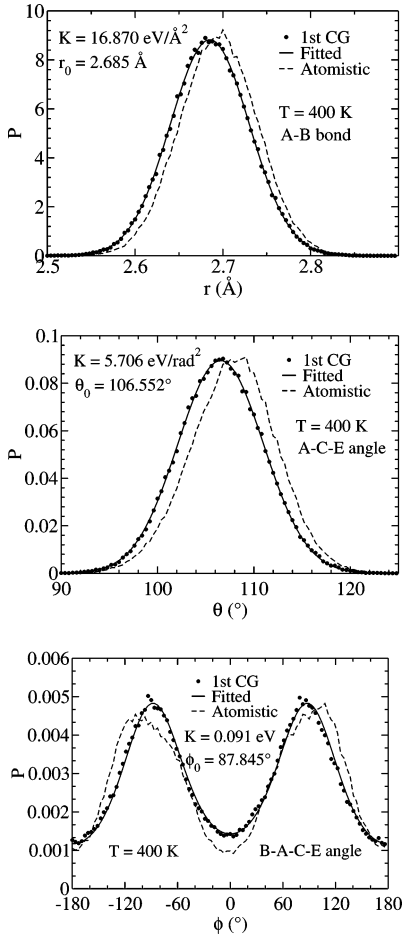

Figure 6. Bond and angle distributions (dotted lines) derived from the first CG run with the fitted parameters from Figure 5 and their fits (solid lines). They deviate from those retrieved from the atomistic run (dashed lines). Only the A−B bond, the A−C−E angle, and the dihedral angle are shown. Others are similar.

as well as the positions, the velocities, and the forces of all atoms, were recorded.

With the partial charge of each CG site fixed as the sum of the respective atomistic partial charges, the FM procedure described in section 2.2 was applied to the 4000 configurations to find the best fit of the short-range nonbonded forces for each pair of CG sites. The forces so obtained were then smoothed using the polynomial expansion in eq 17. In Figure 3 the A−A force before and after smoothing is shown. The other force profiles look similar. The polynomial function is seen to smooth out the noise quite well. The error bars on the curve can be inferred from the spread in the FM data points.

Also seen from Figure 3, there is a small distance $r < r_{\text{core}}$ that cannot be sampled by the FM procedure without some sort of additional enhanced sampling procedure. The FM force field should therefore be somehow extrapolated. The specific choice of the force at $r < r_{\text{core}}$ is expected to have little impact on system properties, so in the present work the force field is assumed to be constant within the core region. The constant force is chosen in such a way that it is neither too large to affect the conservation of total energy because of the finite MD time step interval, nor too small to allow the CG sites to get so deep into the core region that the simulation collapses. Six out of fifteen of the smoothed and extended forces between CG sites are plotted in Figure 4.

From the same atomistic MD configurations used to carry out the force-matching, the distributions of bonds, valence angles, and dihedral angles were computed. The distributions of bonds and valence angles were then fitted with the harmonic functions

$$V(r) = \frac{1}{2}k_r(r - r_0)^2 \tag{23}$$

$$V(\theta) = \frac{1}{2}k_\theta(\theta - \theta_0)^2 \tag{24}$$

while the distribution of the dihedral angle was fitted with the harmonic cosine function

$$V(\phi) = \frac{1}{2}k_\phi(\cos(\phi) - \cos(\phi_0))^2 \tag{25}$$

where k_r, k_θ, and k_ϕ are harmonic constants, r, θ, and ϕ are bond length, valence angle, and dihedral angle, respectively, and r_0, θ_0, and ϕ_0 are their equilibrium positions. The distributions and their fitting functions are plotted in Figure 5. Only the results for the A−B bond, the A−C−E angle, and the dihedral angle are shown, but the others are similar. Note that the exact bonded forces of CG models may not necessarily have the above harmonic functional forms, but the simulations show that these choices of functional forms yield only small errors.

The fitted bonded parameters along with the matched nonbonded forces were then used in the MS−CG model to perform the first CG run. The bond and the angle distributions

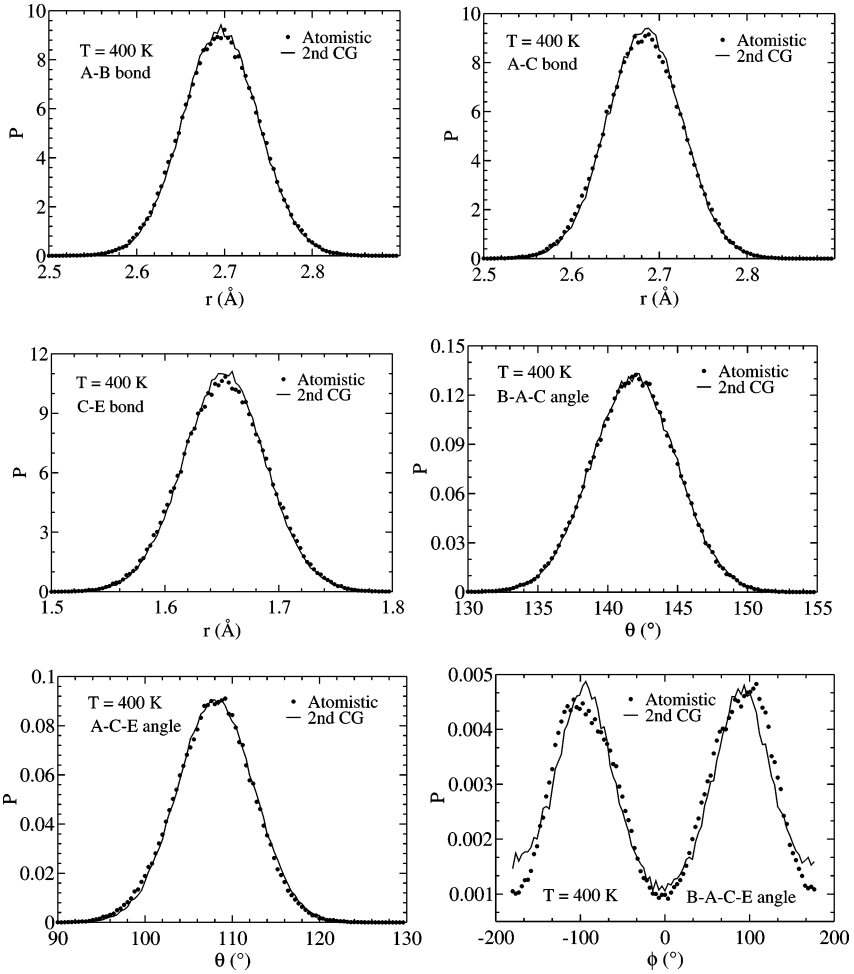

Figure 7. Bond and angle distributions (solid lines) derived from the second CG run with the adjusted parameters. The distributions from the atomistic run (dotted lines) are seen well to be reproduced by the new parameters.

obtained from this CG run were fitted and compared again to the atomistic MD results in Figure 6. It is clearly seen that the originally fitted parameters result in a deviation from the atomistic MD run and therefore require adjustment. According to the method described in section 2.3, the bonded parameters were adjusted by eq 22. The same adjustments were also applied to the valence and dihedral angle parameters by the transformations

$$k_\theta^{\,0} = (k_\theta^{\,1})^2/k_\theta^{\,2}, \quad \theta_0^{\,0} = 2\theta_0^{\,1} - \theta_0^{\,2} \tag{26}$$

and

$$k_\phi^{\,0} = (k_\phi^{\,1})^2/k_\phi^{\,2}, \quad \phi_0^{\,0} = 2\phi_0^{\,1} - \phi_0^{\,2} \tag{27}$$

The superscripts have the same meaning as in eq 22. The adjusted bonded parameters were then put into the MS−CG model to perform the second CG run. The bond and angle distributions obtained from the latter run are compared with those from the original atomistic MD simulation in Figure 7. It is seen that the distributions in the second CG run are almost identical with those from the atomistic run. These results suggest that the method of deriving bonded CG parameters described in section 2.3 is complete and accurate.

The same procedure was also applied to the 64 ion pair system at $T = 700$ K to get the bonded CG parameters and the nonbonded CG potentials at that temperature. The time step of the atomistic run was restrained to be even smaller, 0.36 fs, because of the electronic polarizability at the higher temperature.

TABLE 1: Bonded Force Field Parameters for the CG Models of $EMIM^+NO_3^-$ at $T = 400$ and 700 K.

	T = 400 K		T = 700 K	
bond/angle	K	$r_0/\theta_0/\phi_0$	K	$r_0/\theta_0/\phi_0$
A−B bond	18.282 eV/Å	2.705 Å	17.960 eV/Å	2.700 Å
A−C bond	19.050 eV/Å	2.694 Å	18.048 eV/Å	2.688 Å
C−E bond	25.814 eV/Å	1.658 Å	24.319 eV/Å	1.657 Å
B−A-C angle	12.054 eV/rad^2	142.383°	12.604 eV/rad^2	142.109°
A−C-E angle	5.921 eV/rad^2	109.446°	6.195 eV/rad^2	109.276°
Dihedral angle	0.088 eV	97.806°	0.120 eV	94.800°

Since the system equilibrates faster at 700 K, shorter 2×10^6 MD steps were simulated, propagating the system for 720 ps.The parameters of both CG models at these two temperatures will be given in the next subsection.

3.2. CG Models for the Ionic Liquid. The bonded force field parameters of the CG models for the two temperatures are listed in Table 1. Because the parameters at these two temperatures are very close, it may be concluded that the bonded part of the CG model only very weakly depends on temperature.

The nonbonded parameters obtained from the smoothing of spline data according to eq 17 are listed in the Supporting Information. As one might expect, the force field at $T = 700$ K is different from that at $T = 400$ K. One reason for this difference is the previously mentioned anisotropy effect (see eq 19). The orientational distribution $P(\Omega_{ij})$ is temperature dependent, so that at $T = 700$ K, it is closer to a uniform (isotropic) distribution. By contrast, at $T = 400$ K, the planar imidazole ring and the anion structures are more likely to be

parallel. So even if the orientation-dependent mean force $\mathbf{f}^{P}(r_{ij},\Omega_{ij})$ is temperature independent, the isotropic CG force field $f^{P}(r_{ij})$ adopts a dependence on temperature because of $P(\Omega_{ij})$. It is hard to say if $\mathbf{f}^{P}(r_{ij},\Omega_{ij})$ depends on temperature as a result of neglecting the vibrational forces, the constraint of the system virial, or from other sources.

The CG models accelerate the simulation by about 40 times as compared to the polarizable atomistic model for the same MD time step. In addition, the interval for each time step in the CG models can be at least 5 times larger, so the CG model is at least 200 times faster for the same system size. For larger system sizes, this increase in efficiency may be significantly large. Nevertheless, in the following results, for the sake of careful comparison, the same time interval and number of time steps were used for both the CG models and the atomistic MD model.

3.3. Comparison of CG and Atomistic MD Simulations. *a. Structural Properties.* The structural properties were compared by calculating radial distribution functions (RDFs), which are defined as,[36]

$$g(r) = \frac{V}{N_s^2}\left\langle \sum_i \sum_{j\neq i} \delta(\mathbf{r} - \mathbf{r}_{ij}) \right\rangle \tag{28}$$

where V is the system volume, N_s is the total number of sites, $\mathbf{r}$ is the radial distance, $\mathbf{r}_{ij}$ is the distance vector between sites i and j. For ionic liquids, the RDFs have been calculated for cation−cation, anion−anion, and cation−anion pairs. The positions of the cations and the anions have been described by their center-of-mass.

The RDFs for the CG model at $T = 400$ K are shown in Figure 8. The RDFs for both the nonpolarizable and the polarizable atomistic MD models are also shown in the same figure for comparison. The cation−cation and cation−anion RDFs for both atomistic models have some slight differences, and those from the CG model deviate somewhat from them both. For the atomistic cation−cation RDF, the characteristic second peak appearing at about 4 Å is due to the parallel packing of the planar-like cations. The CG model shifts this peak to a larger distance, which is a consequence of the missing anisotropy of the CG site A. The radial inhomogeneity of the atomistic aromatic ring in the cation cannot be fully rebuilt by the isotropic CG site A. The higher peak intensity of the CG model for the cation−anion RDF can be explained by the same argument.

In Figure 8c, the anion−anion RDF for the polarizable model is quite different from the nonpolarizable model, because the large polarizability of the bulky cations changes the distribution of the polarizable anions around them.[7] Except that the first peak is a little higher, which can also be explained by the anisotropy effect for CG site D, the anion−anion RDF from the CG model successfully reconstructs that of the polarizable atomistic MD model. This demonstrates that the MS−CG approach succeeds in this case in incorporating the many-body polarization effects into the effective pair potential.

The RDFs from the polarizable atomistic model and the CG model at $T = 700$ K are compared in Figure 9. At such a high temperature, the characteristic peak in the cation−cation RDF and the plateau in the anion−anion RDF disappear, because the high temperature allows the cations and the anions to move and rotate more randomly, so that the orientational correlation is no longer significant. In other words, the orientational distribution $P(\Omega_{ij})$ in eq 19 is almost uniform, and the simple isotropic CG force $\mathbf{f}^{P}(r_{ij})$ better represents the underlying atomic

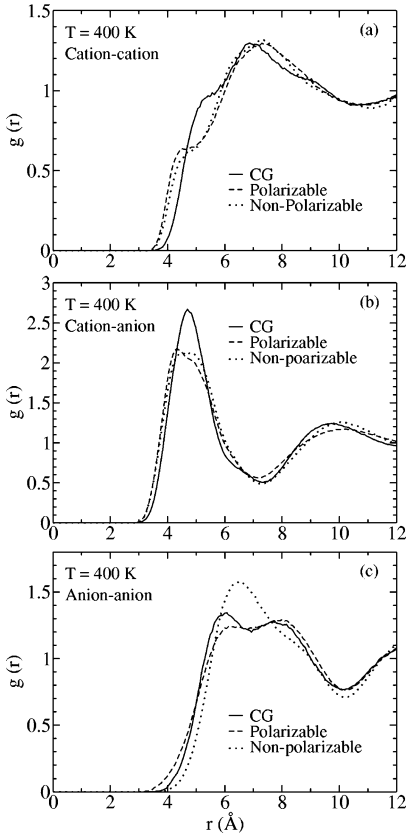

Figure 8. RDFs of 64 ion pairs at $T = 400$ K from the CG model (solid lines), the polarizable atomistic MD model (dashed lines), and the nonpolarizable atomistic MD model (dotted lines).

group than at 400 K. Thus the CG model at $T = 700$ K better predicts the atomistic structure, as illustrated in Figure 9.

The RDFs between individual CG sites at $T = 400$ K were also computed and compared to those from the polarizable atomistic MD simulation. The results are shown in Figures12−14. The Site D-Site D plot is not shown because it is the same as the anion−anion RDF shown in Figure 8c. The bonded peaks are almost identical for both models, so in the figures they are truncated to better demonstrate the nonbonded parts. It can be seen that the CG site−site RDFs are closer to the polarizable atomistic MD results than the cation−cation center-of-mass RDFs. The results for $T = 700$ K are similar and at least as accurate as those for $T = 400$ K.

The CG models at $T = 400$ and 700 K, which were generated using the system with 64 ion pairs, were also applied to systems with the larger sizes of 128, 216, and 400 ion pairs. Only the results for 400 pairs are plotted here because those for 128 and 216 pairs are quite similar. The RDFs are compared with those from the atomistic MD runs. The results at $T = 400$ K are shown in Figure 10, while those at $T = 700$ K are shown in Figure 11. Although at $T = 400$ K the long-range tails of the RDFs from the CG model are a little out of phase with the atomistic MD result, the long-range spatial correlations still exist, with the oscillations extending to 23 Å, or about the half-length of the simulation box. On the other hand, the maxima and the minima of the RDFs are not very far from unity, indicating that the short-range correlations are relatively weak, compared to the inorganic molten salt.[40] The first maximum of the cation−cation RDF is broader and weaker than that of cation−anion RDF, which might be expected from the fact that the ions of ionic liquids are quite bulky.

At $T = 700$ K, the RDFs in Figure 11 from the CG model are again very close to those from the atomistic MD simulation.

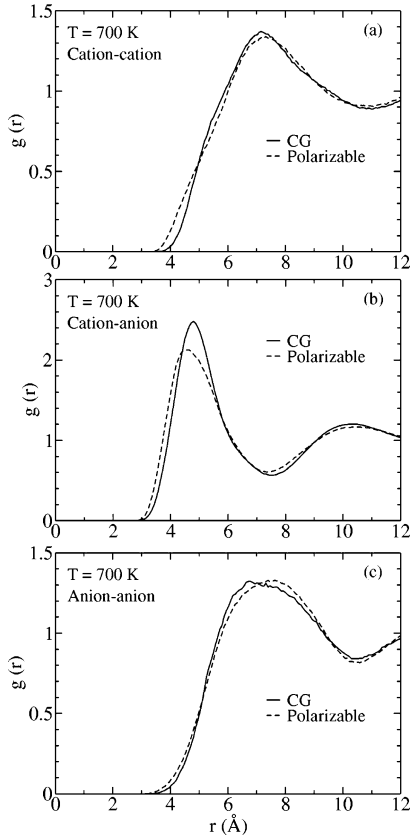

Figure 9. RDFs of 64 ion pairs at $T = 700$ K from the CG model (solid lines) and the polarizable atomistic MD model (dashed lines).

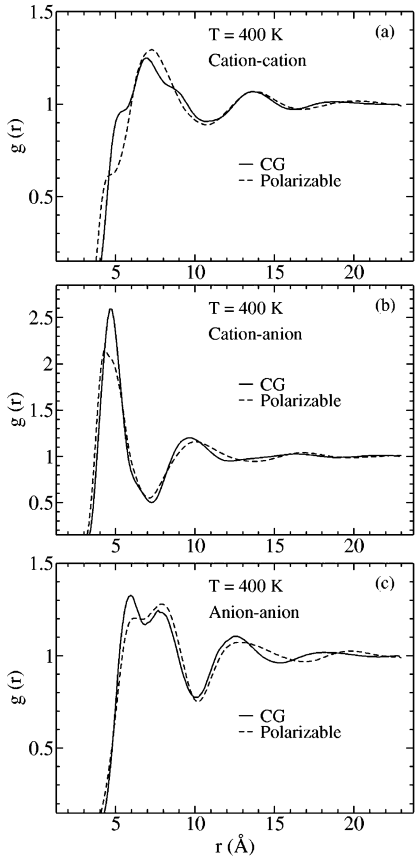

Figure 10. RDFs of the system with the larger size of 400 ion pairs at $T = 400$ K from the CG model (solid lines) and the polarizable atomistic MD model (dashed lines).

Due to higher entropy, the cation−cation and anion−anion RDFs lose their short-range structure and have only one regular peak in the region $r < 10$ Å. The long-range spatial correlations, however, are still present, indicated by the oscillating tails.

b. Thermodynamic Properties. The MS−CG models were also studied in the constant NPT ensemble to test their thermodynamic properties. With the pressure of $P = 1$ atm, for the systems with 64, 128, 216, and 400 ion pairs, the average volumes vs number of ion pairs are plotted in Figure 15. The fitted slopes give the average densities at $T = 400$ and 700 K. The densities from the CG models and the atomistic models are compared in Table 2. The CG models give acceptable errors of 1.2% at 400 K and 4.2% at 700 K. The densities at $T = 400$ K and $P = 100$ atm have also been computed and listed in Table 2.

The isothermal compressibility κ_T at $T = 400$ K can be evaluated from the densities at $P = 1$ atm and $P = 100$ atm, by the expression[41]

$$\kappa_T = -\frac{1}{V}\left(\frac{\partial V}{\partial P}\right)_T = \frac{1}{\rho}\left(\frac{\partial \rho}{\partial P}\right)_T = \left(\frac{\partial \ln(\rho)}{\partial P}\right)_T \approx \left(\frac{\ln(\rho_2/\rho_1)}{P_2 - P_1}\right)_T \quad (29)$$

where V is the system volume and ρ is the system density. Similarly, the thermal expansion coefficient α at $P = 1$ atm can be evaluated from the densities at $T = 400$ K and $T = 700$ K by the expression[41]

$$\alpha = \frac{1}{V}\left(\frac{\partial V}{\partial T}\right)_P \approx -\left(\frac{\ln(\rho_2/\rho_1)}{T_2 - T_1}\right)_P \quad (30)$$

The computed κ_T at $T = 400$ K and α at $P = 1$ atm are listed in Table 2. Despite the fact that the system virial constraint of the MS−CG models depends on temperature (see eqs 14), the data from the MS−CG models are in good agreement with those from the atomistic MD model. Similar to water, which has the experimental values of $\kappa_T = 4.58 \times 10^{-5}$ atm^{-1} and $\alpha = 2.0 \times 10^{-4}$ K^{-1},[42] EMIM$^+$NO$_3^-$ is also a liquid with small compressibility and coefficient of thermal expansion.

From the above results, it can be concluded that the MS−CG models constructed from smaller systems can be used to study larger systems, and with the system virial built in as described in eqs 14, the MS−CG approach gives quite satisfactory thermodynamic properties. The MS−CG approach permits one to systematically construct a CG force field which is able to reproduce both the structural and key thermodynamic properties. Moreover, this method can be equally well applied to systems in which the long-range electrostatics play an important role. These features provide the potential advantages of the method over several previously developed approaches[8−14] for coarse-graining. To our knowledge, this is also the first successful development of a CG model for ionic liquid systems.

4. Conclusions

The MS−CG method has been applied to the polarizable atomistic model of the EMIM$^+$NO$_3^-$ ionic liquid system. The FM method has been used to fit the effective bonded and nonbonded pair interactions separately. By this FM method the many-body polarization effects were also successfully incorporated into effective CG pair interactions. The bonded force field parameters were then refined by retrieving the parameters from the saved atomic MD configurations.

The MS−CG models were run in both the constant NVT and the constant NPT ensembles. They reproduce satisfactory structural properties for different system sizes. With the system

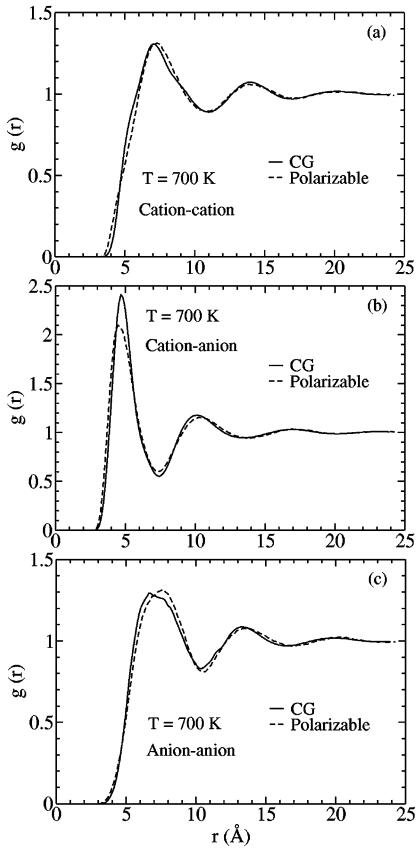

Figure 11. RDFs of the system with the larger size of 400 ion pairs at $T = 700$ K from the CG model (solid lines) and the polarizable atomistic MD model (dashed lines).

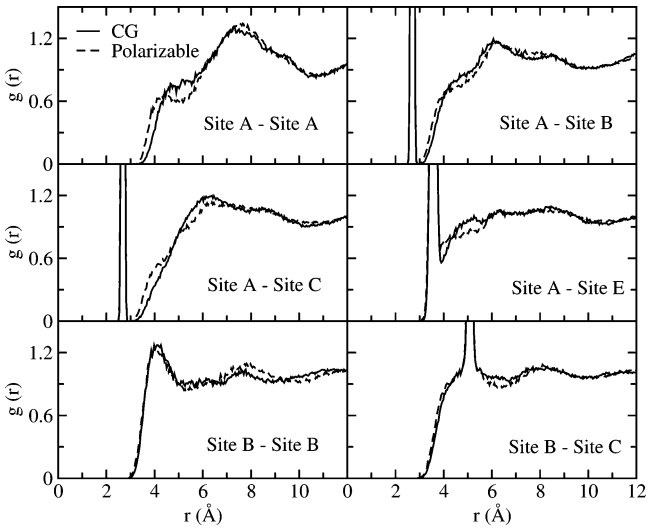

Figure 12. Site−site RDFs between the CG sites at $T = 400$ K compared with the polarizable atomistic MD results.

virial built in, the effective pair interactions retain the system densities and other thermodynamic properties with only small errors at different temperatures. The MS−CG models are at least 200 times faster than the polarizable atomistic MD model.

In the present application of the MS−CG method, the major source of error, which is a general issue of most CG approaches, is the "anisotropy effect", which comes from the approximation that all interactions between CG sites are radially symmetric, namely, orientation-independent. This behavior in CG models arises when the coarse-graining has been particularly "aggressive", i.e., in the present case an entire imidazole ring has been

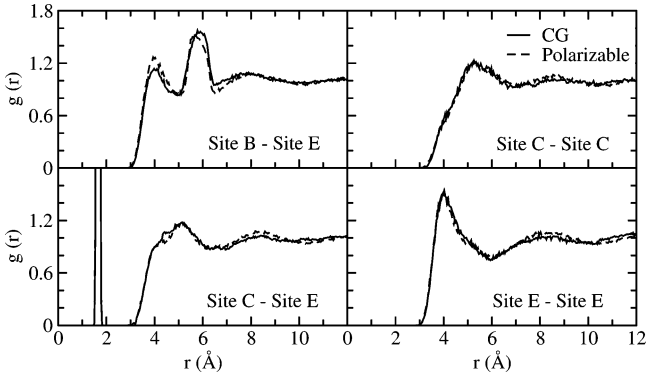

Figure 13. Site−site RDFs between the CG sites at $T = 400$ K compared with the polarizable atomistic MD results. (continued)

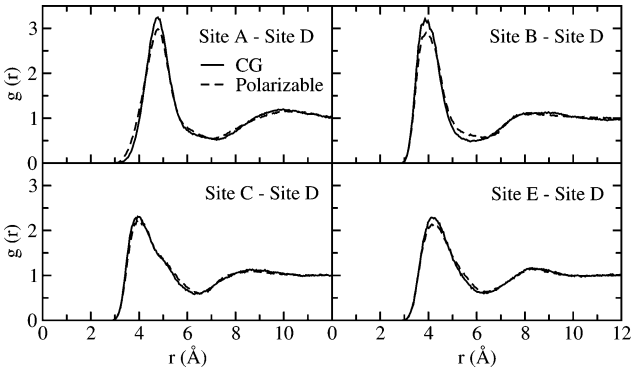

Figure 14. Site−site RDFs between the CG sites at $T = 400$ K compared with the polarizable atomistic MD results. (continued).

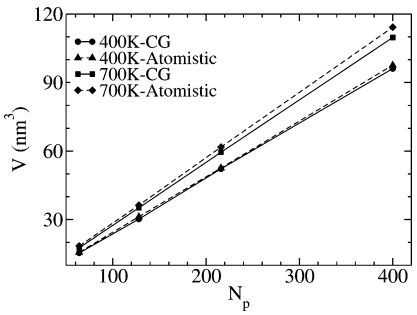

Figure 15. System volume vs. number of ion pairs from the CG models (solid lines) and the polarizable model (dashed lines) at $T = 400$ K and 700 K. The densities are obtained by fitting the slopes of the lines and listed in Table 2.

TABLE 2: Densities ρ (g/cm^3), Isothermal Compressibilities κ_T ($\times 10^{-5}$ Atm^{-1}), and Thermal Expansion Coefficients α ($\times 10^{-4}$ K^{-1}) from the CG Models and the Polarizable Atomistic MD Model

	CG	atomistic
ρ ($T = 400$ K, $P = 1$ atm)	1.1933	1.1791
ρ ($T = 700$ K, $P = 1$ atm)	1.0488	1.0070
ρ ($T = 400$ K, $P = 100$ atm)	1.1977	1.1830
κ_T ($T = 400$ K)	3.7177	3.3355
α ($P = 1$ atm)	4.3025	5.2592

represented by a single CG site. This leads to a relatively small deviation of the liquid CG structures from the atomistic structures and contributes to the reduced transferability of the nonbonded parameters between temperatures. Another possible source of error is that the effective partial charges of the CG sites have been simply set to be the sum of the partial charges of the underlying atoms in the present application. By this approximation the long-range polarizability and the dipole and higher electric moments originating from the finite distribution

of the underlying atoms are approximated by short-range effective pair interactions. This seems to not be a serious problem, as both are weak long-range interactions.

Another general challenge for CG approaches is that the CG sites generally dynamically diffuse faster than the underlying atomistic MD model. This comes from the fact that the interactions between CG sites are effectively site−site potentials of mean force, which do not contain an effective time-dependent frictional forces between the CG sites. This dynamical inconsistency in CG models is the subject of future research in our group.

One of the advantages of the MS−CG method[16,17] is that it constructs the nonbonded interactions systematically from the atomistic MD model and is not limited by a pre-selected function form for these interactions. It is therefore expected to be a good CG approach for other ionic liquids, as well as many other liquid state systems.[16,17] These applications are currently also underway in our group.

Acknowledgment. This research was supported by the Air Force Office of Scientific Research (FA9550-04-1-0381). The authors thank Dr. Jian Zhou for useful discussions. Allocations of computer time from the National Center for Supercomputing Applications (NCSA) and the Center for High Performance Computing at the University of Utah are gratefully acknowledged.

Supporting Information Available: Force field parameters, partial charges, and atomic polarizabilities for the atomistic MD models and matched nonbonded parameters for the MS−CG models. This material is available free of charge via the Internet at http://pubs.acs.org.

References and Notes

(1) Wasserscheid, P.; Keim, W. *Angew. Chem., Int. Ed.* **2000**, *39*, 3772.
(2) Sangster, M. J. L.; Dixon, M. *Adv. Phys.* **1976**, *25*, 247.
(3) Welton, T. *Chem. Rev.* **1999**, *99*, 2071.
(4) Rogers, R. D.; Seddon, K. R. *Science* **2003**, *302*, 792.
(5) Seddon, K. R. *The International George Papatheodorou Symposium: Proceedings*; Boghosian, S. et al., Eds.; Institute of Chemical Engineering and High-Temperature Chemical Processes: Patras, Greece, 1999.
(6) Yan, T.; Burnham, C. J.; Del Pópolo, M. G.; Voth, G. A. *J. Phys. Chem. B* **2004**, *108*, 11877.
(7) Yan, T.; Burnham, C. J.; Voth, G. A. in preparation.
(8) Marrink, S. J.; de Vries, A. H.; Mark, A. E. *J. Phys. Chem. B* **2004**, *108*, 750.
(9) Stevens, M. J.; Hoh, J. H.; Woolf, T. B. *Phys. Rev. Lett.* **2003**, *91*, 188102.
(10) Neilsen, S. O.; Lopez, C. F.; Srinivas, G.; Klein, M. L. *J. Phys.: Condens. Matter* **2004**, *16*, R481.
(11) Meyer, H.; Biermann, O.; Faller, R.; Reith, D.; Müller-Plathe, F. *J. Chem. Phys.* **2000**, *113*, 6264.
(12) Shelley, J. C.; Shelley, M. Y.; Reeder, R. C.; Bandyopadhyay, S.; Klein, M. L. *J. Phys. Chem. B* **2001**, *105*, 4464.
(13) Head-Gordon, T.; Stillinger, F. H. *J. Chem. Phys.* **1993**, *98*, 3313.
(14) Garde, S.; Ashbaugh, H. S. *J. Chem. Phys.* **2001**, *115*, 977.
(15) Murtola, T.; Falck, E.; Patra, M.; Karttunen, M.; Vattulainena, I. *J. Chem. Phys.* **2004**, *121*, 9156.
(16) Izvekov, S.; Voth, G. A. *J. Phys. Chem. B* **2005**, *109*, 2469.
(17) Izvekov, S.; Voth, G. A. *J. Chem. Phys.* **2005**, *123*, 134105.
(18) Izvekov, S.; Parrinello, M.; Burnham, C. J.; Voth, G. A. *J. Chem. Phys.* **2004**, *120*, 10896.
(19) Izvekov, S.; Voth, G. A. *J. Phys. Chem. B* **2005**, *109*, 6573.
(20) Hone, T. D.; Izvekov, S.; Voth, G. A. *J. Chem. Phys.* **2005**, *122*, 54105.
(21) Urahata, S. M.; Ribeiro, M. C. C. *J. Chem. Phys.* **2004**, *120*, 1855.
(22) Del Pópolo, M. G.; Voth, G. A. *J. Phys. Chem. B* **2004**, *108*, 1744.
(23) Margulis, C. J.; Stern, H. A.; Berne, B. J. *J. Phys. Chem. B* **2002**, *106*, 12017.
(24) Morrow, T. I.; Maginn, E. J. *J. Phys. Chem. B* **2002**, *106*, 12807.
(25) Sprik, M. *J. Phys. Chem.* **1991**, *95*, 2283.
(26) Car, R.; Parrinello, M. *Phys. Rev. Lett.* **1985**, *55*, 2471.
(27) Ercolessi, F.; Adams, J. B. *Europhys. Lett.* **1994**, *26*, 583.
(28) De Boor, C. *A Practical Guide to Splines*; Springer-Verlag: New York, 1978.
(29) Akkermans, R. L. C.; Briels, W. J. *J. Chem. Phys.* **2000**, *113*, 6409.
(30) Straus, J. B.; Voth, G. A. *J. Chem. Phys.* **1992**, *96*, 5460.
(31) Tschöp, W.; Kremer, K.; Batoulis, J.; Bürger, T.; Hahn, O. *Acta Polym.* **1998**, *49*, 61.
(32) Fukunaga, H.; Takimoto, J.; Doi, M. *J. Chem. Phys.* **2002**, *116*, 8183.
(33) Nielsen, S. O.; Lopez, C. F.; Srinivas, G.; Klein, M. L. *J. Chem. Phys.* **2003**, *119*, 7043.
(34) Cang, H.; Li, J.; Fayer, M. D. *J. Chem. Phys.* **2003**, *119*, 13017.
(35) Dl_poly user manual. Forester, T. R.; Smith, W.; CCLRC, Daresbury Laboratory, Daresbury, Warrington, UK, 1995.
(36) Allen, M. P.; Tildesley, D. J. *Computer Simulation of Liquids*; Clarendon Press: Oxford, 1987.
(37) Hoover, W. G. *Phys. Rev. A* **1985**, *31*, 1695.
(38) Melchionna, S.; Ciccotti, G.; Holian, B. L. *Mol. Phys.* **1993**, *78*, 533.
(39) Cornell, W. D.; Cieplak, P.; Bayly, C. I.; Gould, I. R.; Merz, K. M.; Ferguson, D. M.; Spellmeyer, D. C.; Fox, T.; Caldwell, J. W.; Kollman, P. A. *J. Am. Chem. Soc.* **1995**, *117*, 5179.
(40) Violette, R. A. L.; Budzien, J. L.; Stillinger, F. H. *J. Chem. Phys.* **2000**, *112*, 8072.
(41) Walser, R.; Mark, A. E.; van Gunsteren, W. F. *J. Chem. Phys.* **2000**, *112*, 10450.
(42) Franks, F., Ed. *Water: a comprehensive treatise*; Plenum: New York, 1972.